Renewable Energy 34 (2009) 2437–2446

Contents lists available at ScienceDirect

Renewable Energy

journal homepage: www.elsevier.com/locate/renene

Modeling and simulation of the pioneer 1 MW solar thermal central receiver system in China

Zhihao Yao [a], Zhifeng Wang [a,*], Zhenwu Lu [b], Xiudong Wei [b]

[a] Key Laboratory of Solar Thermal Energy, Photovoltaic System of Chinese Academy of Sciences, Institute of Electrical Engineering, Beijing 100190, China
[b] Changchun Institute of Optics, Fine Mechanics and Physics, Chinese Academy of Sciences (CAS), Jilin 130033, China

A R T I C L E I N F O

Article history:
Received 14 September 2008
Accepted 22 February 2009
Available online 24 March 2009

Keywords:
Central receiver system (CRS)
DAHAN
HFLD
Heliostat
Receiver
Simulation

A B S T R A C T

DAHAN, the pioneer 1 MWe CRS (central receiver system) funded by Ministry of Sciences and Technology (MOST), which can be regarded as the milestone in solar thermal power development in China, is now under construction at the foot of The Great Wall nearby Beijing. The major objective of the design and construction of DAHAN is to demonstrate the operation of CRS in China. A software tool HFLD is developed for heliostat field layout design and performance calculation. The simulation results from HFLD approximately agree very well with the published heliostat field efficiency data from Spain PS10. Based on that, the heliostat field layout of DAHAN is designed using HFLD and the whole CRS performance is simulated in the TRNSYS plant model. The modeling and simulation of this plant is presented in this paper.

1. Introduction

As well known, electric power consumption in China has been increasing greatly with the rapid economic development. Its total installed capacity of electric power has achieved 700 GW by the end of 2007 while it's predicted to reach 900 GW in 2010 [1]. Due to prediction, China will have the world's largest installed power capacity of 1186 GW by 2020. The rapid increase in energy demand and threatening climate change have both urged China to change its current electric power structure with coal power amount accounting nearly 75%. Actually, two-thirds of China's territory has over 2200 annual hours' sunshine. The abundant desert and Gobi areas in North-West China hold enormous potential for large-scale deployment of solar thermal power systems. Solar thermal power has probably the greatest potential of any single renewable energy area to meet the national power structure adjustment demand and mitigate the greenhouse gas emissions. Rapid development occurred recently in basic technology and market strategy of solar thermal power systems in China. DAHAN, the pioneer 1 MWe CRS, is now under construction at the foot of The Great Wall in Badaling Beijing.

The main objectives of the work concerned in this paper are to evaluate DAHAN power system design and to develop a powerful tool able to simulate and predict its operating results under different conditions.

2. Validation of the heliostat field design tool

The plant mainly consists of Collector System (CS), Receiver System (RS), Thermal Storage System (TSS), Electrical Power Generation System (EPGS) and the Balance of Plant (BOP). When solar irradiation is converted into electrical form, the transfer from beam radiation to thermal energy and then to electricity has to be considered thoroughly. Usually CS cost accounts nearly 50% of the total plant capital investment. So the heliostat field efficiency improvement plays an important role on the cost reduction potential of such solar thermal power.

Several codes including UHC, DELSOL, HFLCAL, MIRVAL, FIAT LUX and SOLTRACE have been developed for heliostat field layout design and concentrated solar flux calculation since 1970s. However, much works are needed to adapt those codes to specific features and specific needs of different projects [2]. Thus, researchers from CAS developed the code HFLD which is designed to optimize the heliostat field layout on costs criteria, to establish heliostat field efficiency matrixes, to determine flux maps on receiver aperture, and to predict instantaneous or annual performances of the central receiver system. It has some features in common with the codes quoted above.

* Corresponding author. Tel.: +86 10 62558289; fax: +86 10 62587946.
E-mail address: zhifeng@vip.sina.com (Z. Wang).

0960-1481/$ – see front matter © 2009 Elsevier Ltd. All rights reserved.
doi:10.1016/j.renene.2009.02.022

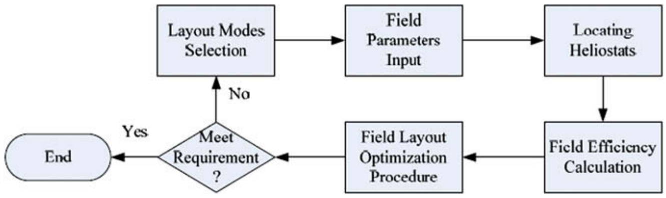

Fig. 1. The basic calculation flow chart of HFLD.

Table 1
Comparison between PS10 data published and HFLD calculation results.

PS10 heliostat field efficiency	Data published	HFLD	Error
Nominal field efficiency	77%	76.5%	−0.5%
Annual mean field efficiency	64%	64.07%	+0.07%
Annual mean cosine efficiency	>81%	82.3%	<+1.3%
Annual mean shading & blocking efficiency	>95.5%	92.9%	>−2.6%
Annual mean atmospheric transmittance	95%	95.01%	+0.01%
Rated power transferred	55.0 MWt	56.3 MWt	+1.3 MWt

Monte Carlo method is implemented here to provide ray vectors onto the receiver aperture and flux distribution after calculation is described statistically. Various no-blocking heliostat field layouts are available in this tool besides the conventional ones. The tower height, receiver tilt angle and its aperture sizes, heliostats number and dimensions are designed as user inputs. Heliostat field performance is subject to disturbances from mirror and tracking error sources which mainly include: azimuth rotational axis tilt, mirror alignment or canting nonorthogonality relative to the heliostat centerline, pivot point offset, gravity deflections, azimuth and elevation reference position error, atmospheric refraction, sun position algorithms, drive and control system granularity. For the sake of simplicity, the mirror and tracking errors are assumed to have normal Gaussian distributions in the HFLD heliostat model. In the shading and blocking losses calculation model, the ray tracing method is used where $m \times n$ points on each mirror's surface are traced. For calculation of the reflected beam intercepted by the receiver aperture, the sunlight beam projected onto a point of the mirror surface is approximated as a cone with cone angle $\varepsilon = 9.3$ mrad. The cone's symmetric axis coincides with the incident direction and several rays are traced in the cone. In order to improve the land utilization, the shadow effect caused to the plants growing around the heliostats is also calculated in HFLD. The merit function for heliostat field optimization is as equation (1). The calculation flow chart of HFLD is shown in Fig. 1.

$$F_{merit} = \frac{1}{field\ density \times annual\ efficiency} \tag{1}$$

Coordinates of the 624 heliostats installed in PS10 and the local geographical data are input to HFLD for its performance validation. The results agree well with PS10 field data published (Fig. 2, Table 1) [3]. For the lack of information in details, the deviations of HFLD calculation results from PS10 data can be explained as follows:

1. There is a small slope angle of the PS10 heliostat field terrain but it's assumed to be totally flat in the HFLD calculation [4].
2. The calculation time step, the start and end hours of each day and the mirrors' ray trace interval setting used in PS10 are unknown.
3. The radiation model adopted in PS10 calculation maybe a little different from what is assumed in HFLD. It will result in the deviation of power transferred.

Based on that, the DAHAN field layout is designed using HFLD and the whole CRS is modeled and simulated in TRNSYS. The modeling and simulation of this plant is presented below.

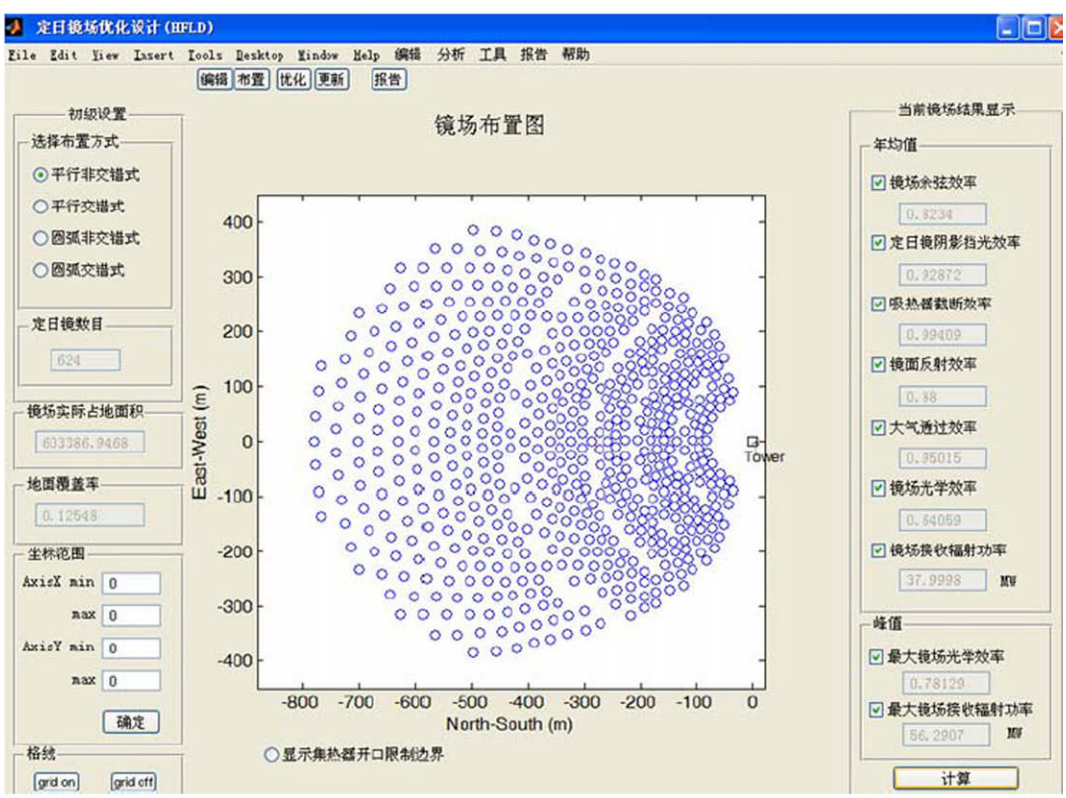

Fig. 2. Visualization of PS10 calculation results from HFLD.

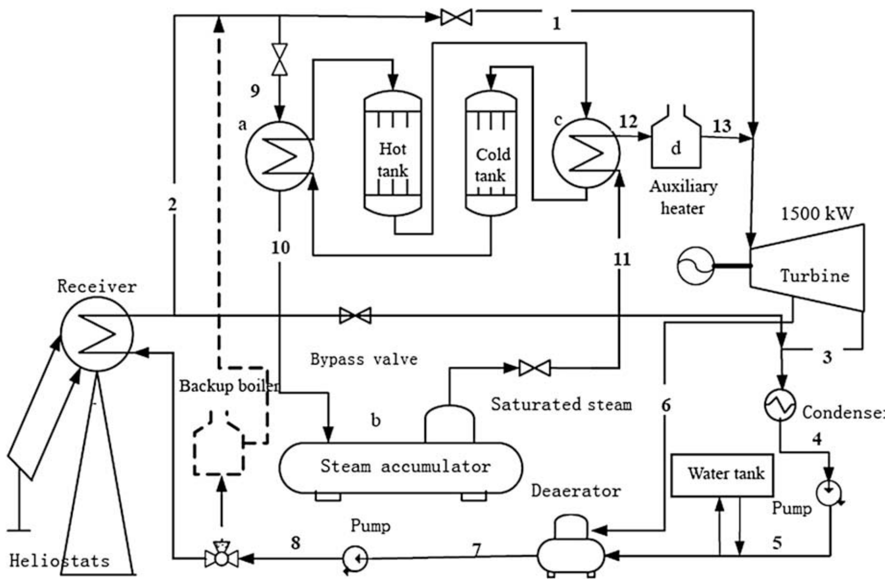

Fig. 3. Schematic of the DAHAN central receiver system.

3. Mathematical model description of DAHAN system

A schematic of the DAHAN plant under construction is shown in Fig. 3. The system mainly makes use of a field of heliostats, superheated steam cavity receiver and turbine, thermal storage in oil and water/steam. Sunlight is reflected from a field of tracking heliostats and concentrated onto the receiver, which heats up the feedwater to superheated steam, flows back down to grade level, and is sent to turbine inlet directly or stored in the storage system. Oil is pumped from the cold tank to the hot tank through the charging heat exchangers and heated with steam produced by the receiver. Auxiliary heater is available before turbine inlet when saturated steam is extracted from accumulator and heated by oil from hot tank.

Though much experience handling oils and molten salt exist in the petrochemical and heat treating industry, the storage system combined of a two-tank oil storage with a saturated steam flash storage tank is preferred to the two-tank salt or pure oil storage. As at the present stage of CRS development in China, it is considered a key point for DAHAN project the first successful demonstration system at low cost and low risk in operation.

Mathematical models of real processes cannot take all aspect of reality into account. Simplifying assumptions have to be made and models are only approximations of reality. The first step in developing a model is to determine the process variables that are relevant in the behavior of the plant. The second step is the analysis of the way in which the variables are dynamically related. The whole plant's energy balance model with the main related process variables is shown in Fig. 4. Power losses of different models for each time step are calculated from the models described below [5].

3.1. Modeling of heliostat field

The configuration of the heliostat field and the tower can take two basic forms: a surround field and a north field. Since northern heliostats have a better view of the sun, the north field configuration has a greater optical efficiency than the surround field configuration at low plant design power levels [6]. To this 1 MWe range CRS, the north field form is considered. Decisions regarding the best position for locating heliostats relative to the receiver and

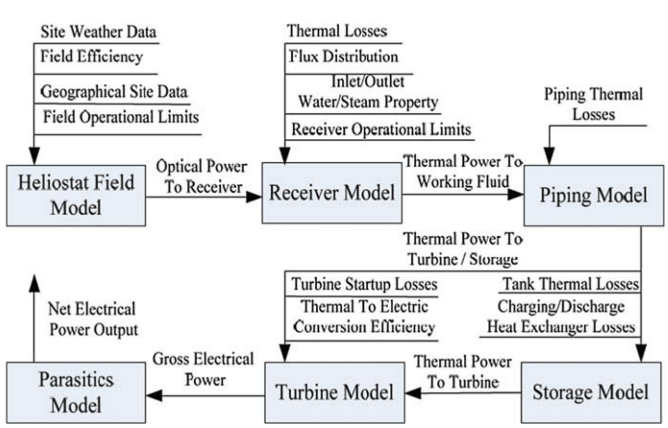

Fig. 4. Power flow diagram for DAHAN.

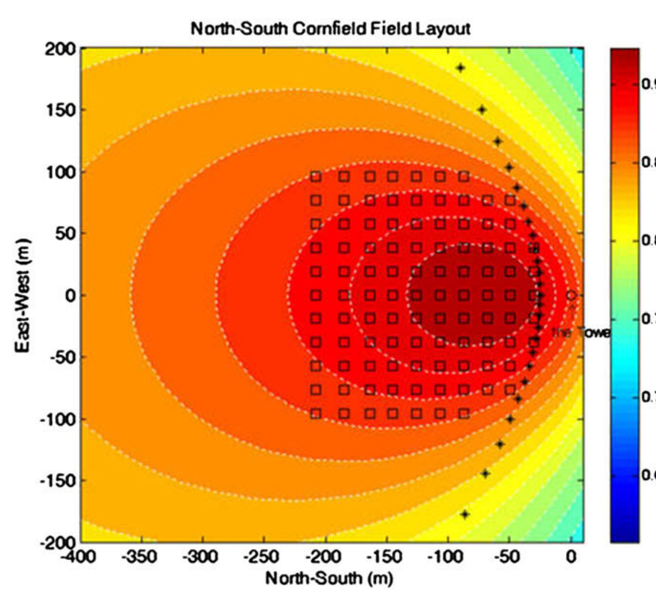

Fig. 5. North-South cornfield layout.

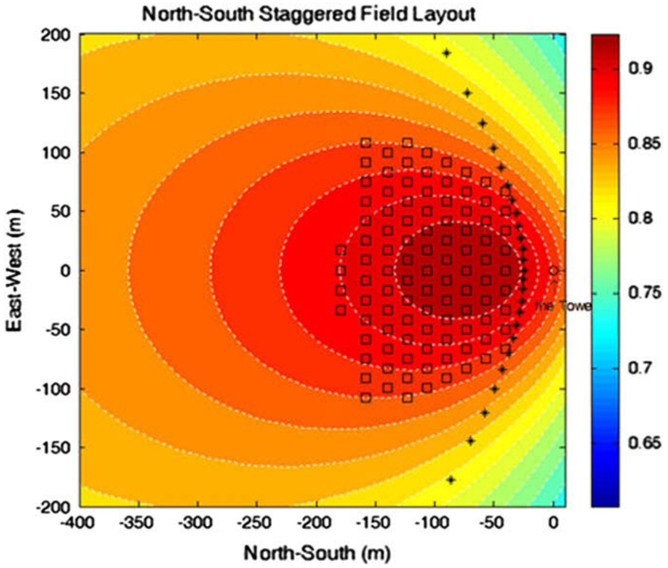

Fig. 6. North-South staggered layout.

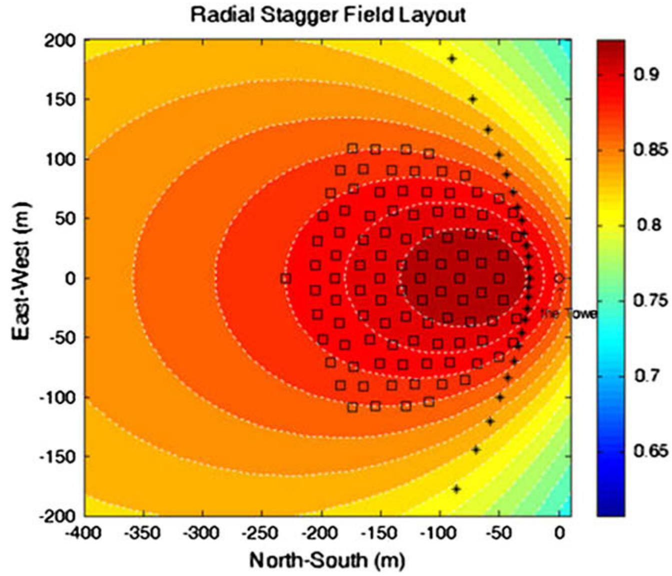

Fig. 8. Radial staggered layout.

how high to place the receiver above the field constitute a multi-faceted problem, in which the land cost and various heliostat power loss mechanisms are the main variables.

These mechanisms include losses due to:

Projected reflection area being lower than total reflective area (cosine losses, $\eta_{\cos}$); blocking of incident sunlight by adjacent heliostats, η_{block}; shading of reflected sunlight by adjacent heliostats,η_{shadow}; atmospheric attenuation of reflected sunlight, η_{atten}; mirror reflectivity, η_{refl}; and reflected light that misses the receiver (spillage efficiency, η_{spill}) due to heliostat errors and aiming strategies. For accurate prediction of the thermal performance of a CRS, it's necessary to define the flux profile produced on the receiver by a large number of representative heliostats throughout each day of a typical year. In HFLD, this is done by the use of ray tracing and mathematical simulation techniques to determine the overall field efficiency which is expressed as equation (2) [7]:

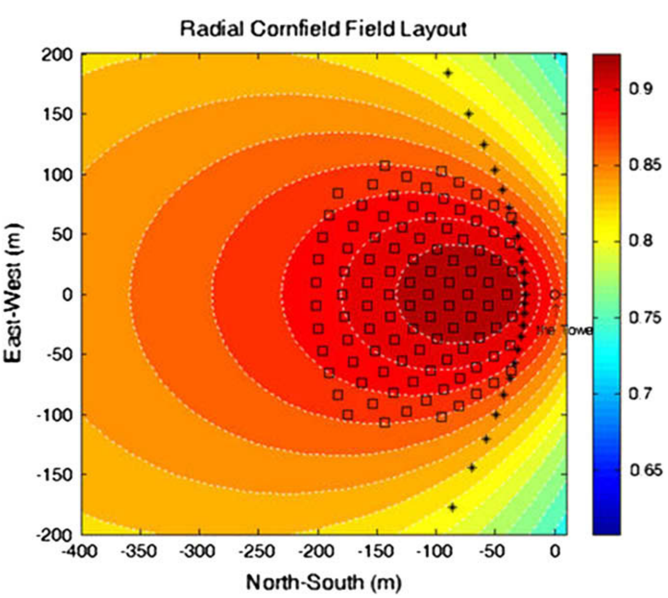

Fig. 7. Radial cornfield layout.

$$\eta_{field} = \eta_{\cos} \cdot \eta_{shadow} \cdot \eta_{block} \cdot \eta_{refl} \cdot \eta_{atten} \cdot \eta_{spill} \tag{2}$$

Four types of suggested fields specified as North-South cornfield layout, North-South staggered layout, Radial cornfield layout and Radial staggered layout as shown in Figs. 5–8 were analyzed optically in the design of DAHAN. The annual average field zone efficiency distribution calculated from heliostat by heliostat and the layout boundary limited by the receiver aperture's projection on the ground are both shown as well. Assumptions that all mirror surfaces have ideal spherical curvature and tracking error is within acceptable range are made. The parameters used for the heliostat field layout and optimization are listed in Table 2. Comparison results of these four layouts' yearly field efficiency change are shown in Fig. 9. The value plotted by the curve is the daily average field efficiency. The reason for the behavior of the curve between day 30–50 and day 300–320 is that the time step adopted in this calculation is 1 h and shorter time step is suggested to avoid the sharp break points. According to the optimization algorithm proposed in HFLD by Eq. (1), it can be found that the North-South staggered type (Fig. 6) is preferred for its low land cost and high annual efficiency. Numerical values calculated from this type's annual average performance are as follows: $\eta_{\cos} = 0.863$, $\eta_{block} \cdot \eta_{shadow} = 0.942$, $\eta_{refl} = 0.876$, $\eta_{atten} = 0.976$, $\eta_{spill} = 0.966$, then $\eta_{field} = 0.671$. The total land coverage for this type is 25,874.96 m^2, so the field density is 0.386.

The efficiency matrix shown in Fig. 10 gives the heliostat field efficiency for a number of pairs of solar azimuth and zenith angle. This matrix is linear interpolated using the inputs of the actual solar

Table 2
Parameters for heliostat field layout and optimization.

Parameter	Designed value	Parameter	Designed value
Total heliostat number	100	Each heliostat size	100 m^2
Receiver aperture size	25 m^2	Mirror reflectivity	0.9
Tower height	100 m	Mirror cleanness	0.97
Field cosine boundary	0.842	Terrain slope angle	No angle
Receiver tilt angle	25°	Field latitude	40.4 N
		Field longitude	115.9 E
Tracing points' number for S&B per mirror	2500	Tracing points' number for spillage per mirror	25
Calculation time step	1 h/10 days	Layout mode	No-blocking

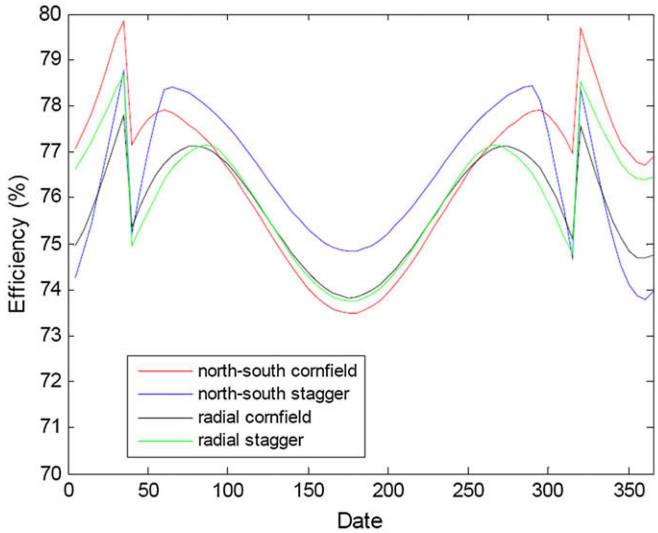

Fig. 9. Annual efficiency comparison of four different heliostat field layouts.

azimuth and elevation angles in TRNSYS plant model [8]. The efficiency is a measurement of how well the heliostat field transfers power to the absorber area of the receiver. The power to the receiver Q_{inc} is evaluated by Equation (3):

$$Q_{inc} = A_{field} \cdot I \cdot \eta_{field} \cdot \Gamma \tag{3}$$

where, total mirror surface $A_{field} = 10,000\ \mathrm{m}^2$ in DAHAN and I is the transient or average direct normal irradiance value depending on the evaluation period, so is the field efficiency, η_{field}; control parameter Γ describing the fraction of the field in track is usually assumed 100%.

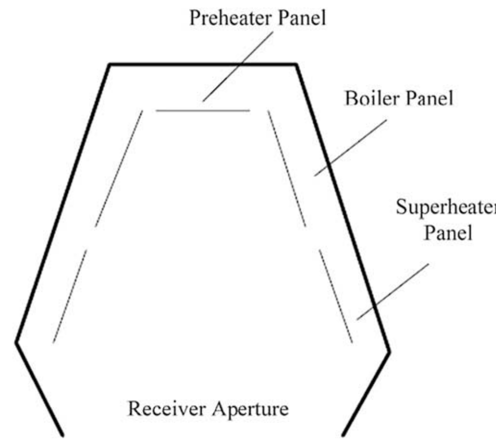

Fig. 11. Schematic of the DAHAN receiver layout.

3.2. Modeling of receiver

The selection of a north field or surround field configuration has great impact on receiver design. In this project, a cavity receiver consisting of preheater panel, boiler and superheater panels as shown in Fig. 11 is designed to meet the selected north field flux concentration requirement. The power absorbed distribution for the normal operation condition is 19.08% for the preheater panel, 65.26% for the boiler panel and 15.66% for the superheater panel. This value is maintained by the control system throughout one day.

A steam drum used as an energy accumulator element that contains water and steam is located between the boiler and

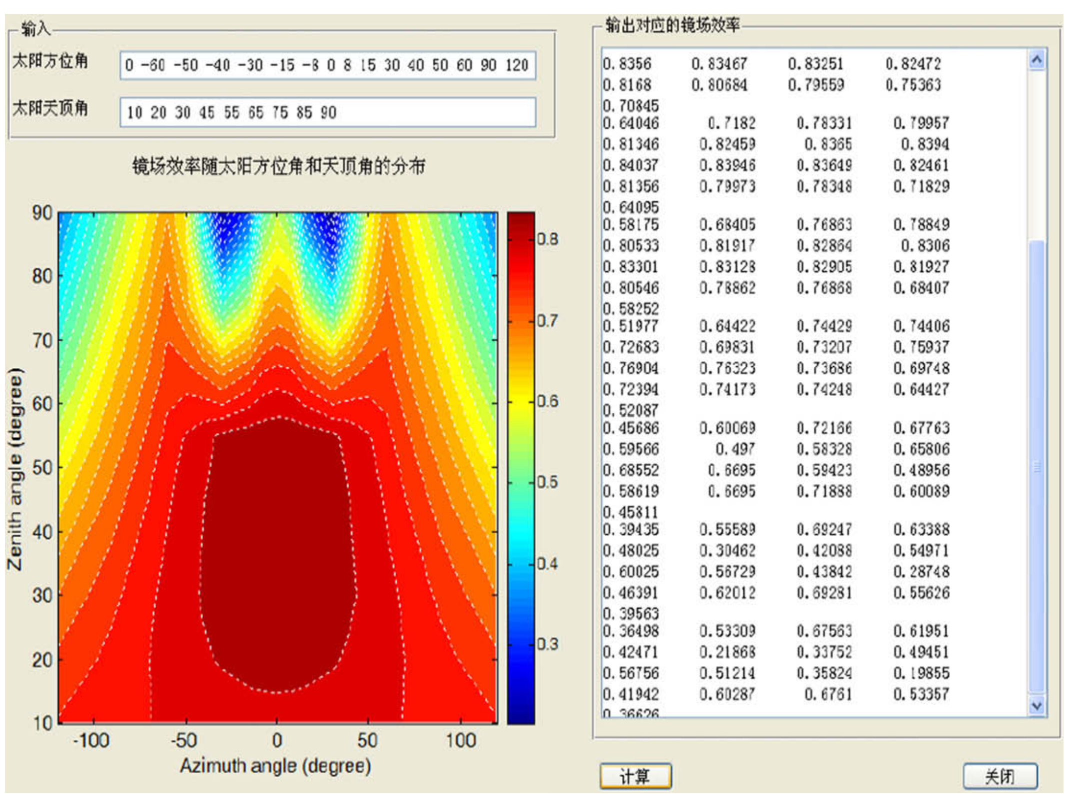

Fig. 10. Heliostat field efficiency matrixes calculated by HFLD.

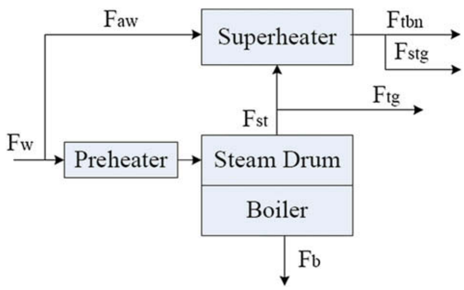

Fig. 12. Receiver mass and energy balance model. Where: Fw = feed water flow; Faw = attemperation water flow; Fb = blow down flow; Fst = saturated steam flow; Ftbn = steam flow to the turbine; Fstg = steam flow to the storage; Ftg = turbine gland steam flow.

superheater section in the water/steam cycle [9]. Water enters the steam drum from the preheater panel and is pumped to the boiler panels where it is converted to steam as illustrated in Fig. 12. Temperature sensors and specific field operation strategy and control system will be tried to overcome the well-known problem of superheating in this pilot central receiver system.

The flux profile projected on the receiver aperture by a designed North-South staggered field from spring equinox noon 12:00 to 15:00 is shown in Figs. 13–16. Water and steam two-phases occur in the receiver's boiler panels when they absorb power transmitted from heliostat field. For fluid's heating, boiling, superheating and receiver thermal losses analysis, the flux distribution variation calculated by HFLD is used. The exact flux density distribution on the absorbing elements is difficult to predict and assumption of power absorbed distribution as mentioned above is made.

The work presented in this paper is focused on the DAHAN CRS simulation based on energy balance. The control system design and its simulation related with thermal and electrical transient process are not considered here. So the individual thermal losses including conduction losses, emission losses, convection losses and reflection losses need to be evaluated in the receiver simulation model. The emission and convection losses account most of the receiver thermal losses resulting from calculation. In the receiver model used in TRNSYS, the conductive losses are neglected in the calculation of the net absorbed power [8]:

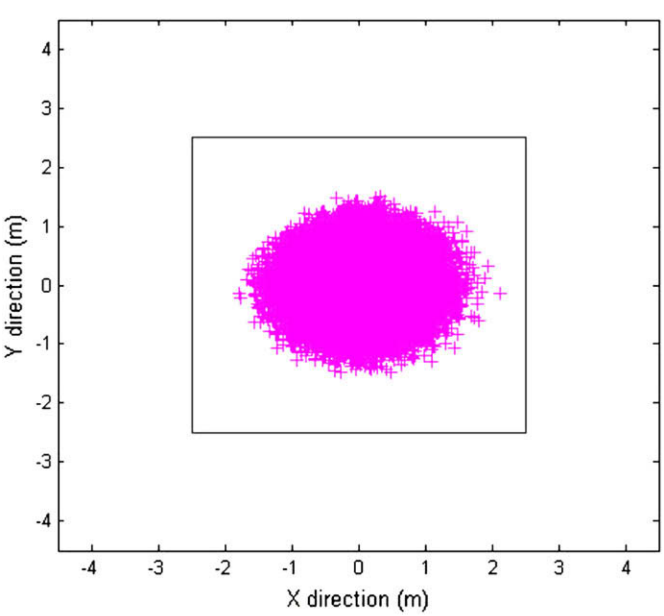

Fig. 13. Focus shape at 12:00.

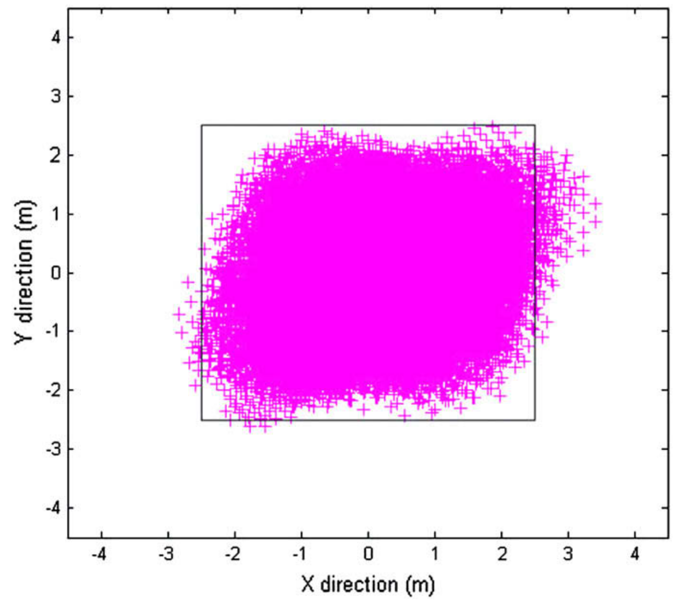

Fig. 14. Focus shape at 15:00.

$$\dot{Q}_{net} = \alpha\dot{Q}_{inc} - \dot{Q}_{conv} - \dot{Q}_{emi} \quad (4)$$

where, $\dot{Q}_{net}$ is the net absorbed power; $\dot{Q}_{inc}$ is the incident power into the receiver aperture from the heliostat field; $\dot{Q}_{conv}$ is the convection loss; $\dot{Q}_{emi}$ is the radiation loss; α is the absorptivity which assumed to be 0.97 here considering the re-reflection within the cavity.

The magnitude of different thermal losses varies, and it depends on the receiver type, geometry and size. The standard heat transfer literature did not provide correlations for the range of conditions in which solar receivers operate. Measurements of those losses are very difficult for the experimental methods are typically limited to the determination of total thermal loss. In calculation of convection losses, the recommended procedure of Siebers and Kraabel which has gained the most acceptance among receiver designers and analysts is followed [10]. The recommended correlations as follow are used here:

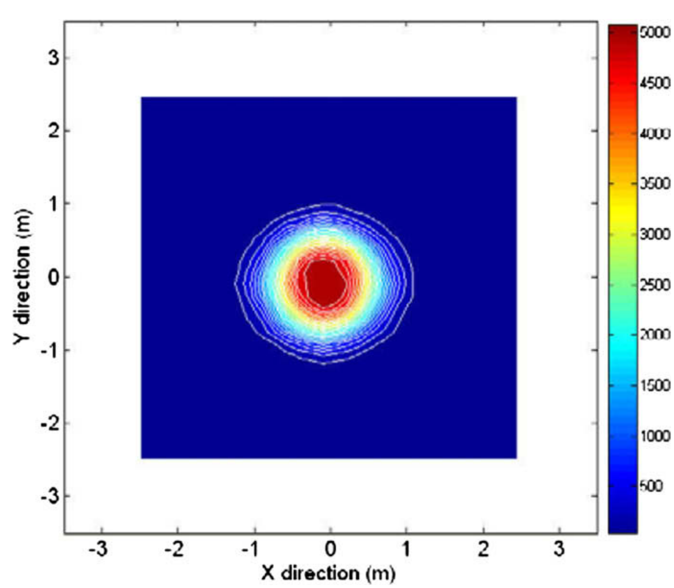

Fig. 15. Flux density at 12:00.

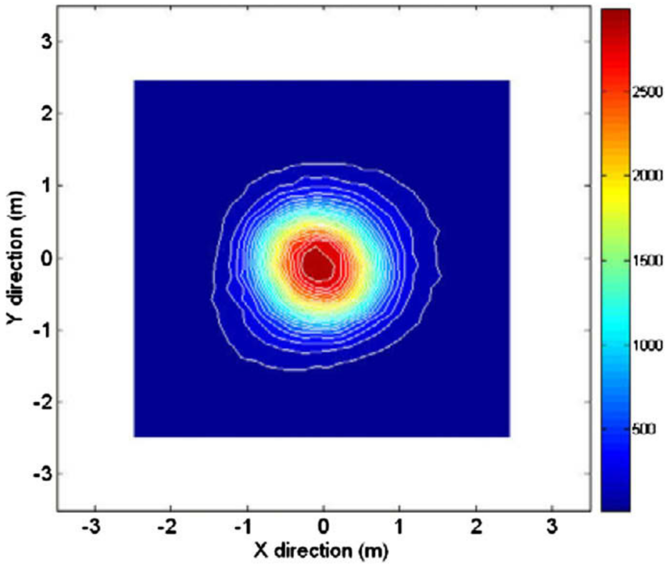

Fig. 16. Flux density at 15:00.

$$h_{nc} = 0.81(T_w - T_a)^{0.426} \quad (5)$$

$$h = \left(h_{fc}^a + h_{nc}^a\right)^{1/a} \quad (6)$$

$$\dot{Q}_{conv} = hA(T_w - T_a) \quad (7)$$

where, h_{nc} is the natural convection coefficient; h_{fc} is the forced convection coefficient but not well understood yet, so it's assumed to be equal to h_{nc} for simplification here; a is an exponent derived empirically and equal to 1.0 here for the cavity receiver as recommended by literature [10]; h is the forced and natural combined convection coefficient; A is the receiver surface area and equal to 40 m^2; T_w is the mean receiver wall temperature and assumed to be 430 °C at normal operation here; T_a is the ambient temperature and assumed to be 25 °C.

Simplification is made to estimate emission losses from the central receiver [11]:

$$\dot{Q}_{emi} = \sigma\varepsilon A_a\left(T_w^4 - T_a^4\right) \quad (8)$$

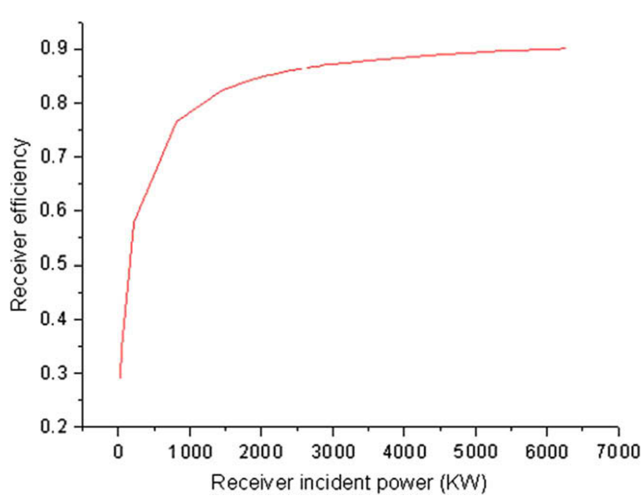

Fig. 17. Calculated receiver efficiency versus incident power.

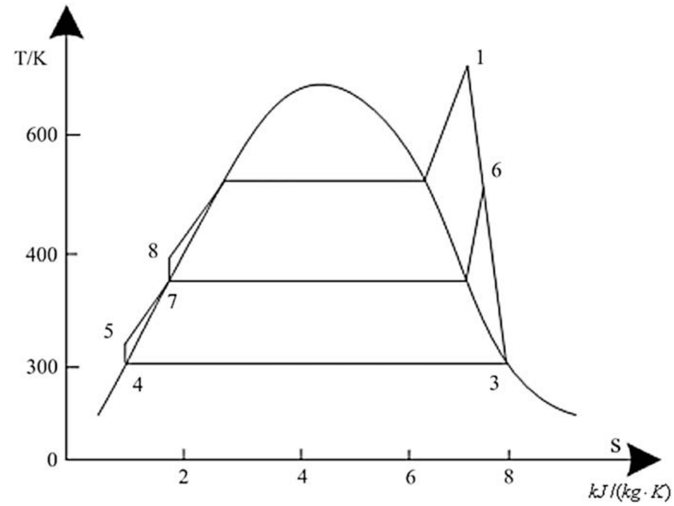

Fig. 18. Temperature–entropy (*T–s*) schematic diagram of power cycle.

where, $\sigma = 5.67 \times 10^{-8}$ W/(m^2 K^4); ε is the emissivity and assumed to be 0.88 here; A_a is the receiver aperture area and equal to be 25 m^2 here.

The curve of receiver efficiency versus incident radiant power $\dot{Q}_{inc}$ is thus calculated as shown in Fig. 17. This is based on flux distribution calculated by HFLD, the various receiver thermal losses analysis in above and its comparison to some experienced cavity water/steam receiver models such as CESA-I [9]. For evaluation of energy conversion, such approximation is acceptable. More accurate function will be available when actual measurements are obtained.

It calculates the demanded mass flow rate $\dot{M}$ of the heat transfer fluid to achieve a user-defined receiver outlet temperature T_{out} by Equation (9):

$$\dot{M} = \frac{\dot{Q}_{net}}{h_{out} - h_{in}} = \frac{\dot{Q}_{net}}{c_p(T_{out} - T_{in})} \quad (9)$$

where, T_{out} is the receiver outlet steam temperature with outlet enthalpy h_{out} and T_{in} is the receiver inlet water temperature with inlet enthalpy h_{in}; c_p is the specific heat of fluid.

3.3. Modeling of power cycle

The power cycle used in the DAHAN plant is a conventional Rankine cycle. The Rankine cycle in the system simulation model mainly consists of high and low pressure turbine stages with controller and bypass loop, feed water heaters, deaerator and condenser. In this low capacity of 1 MWe Rankine cycle, only one steam extraction outlet from turbine is designed to meet the water preheating requirement. A temperature–entropy schematic diagram of the power cycle with all corresponding intermediate state points at the design main operation mode is shown in Fig. 18.

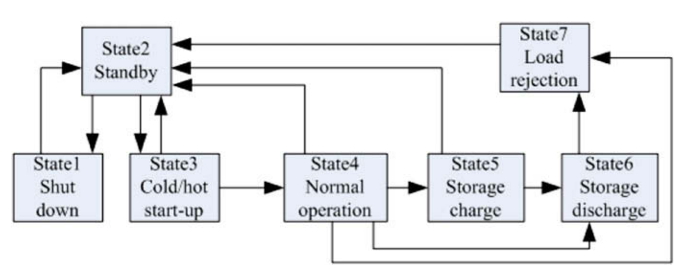

Fig. 19. Transitions between the plant operation states.

Thermal Storage System (TSS) allows power generation to be shifted to periods of peak demand and provides a buffer between the plant's receiver and turbine, allowing the turbine to operate during cloud-induced transients. There are three approaches for storing thermal energy have been considered over the years for solar thermal systems. These are sensible-heat storage (where a change of temperature occurs), latent heat storage (where a change of phase occurs) and thermo-chemical energy storage (where a reversible chemical reaction takes place) [7]. Synthesized silicate oil and pressurized water/steam are chosen as the high and low temperature thermal storage medium here. It can reduce the TSS cost for the expensive oil only stores part of the sensible-heat from superheated steam.

The plant's operation strategy is designed as the following conditions generally:

State 1: Shut down of the plant when there is no sufficient thermal energy to feed the turbine; the heliostats are in the stow position;
State 2: Standby, all the heliostats are focused on the imaginary standby aim points and the receiver is not in operation;
State 3: Cold and hot start-up;
State 4: Normal operation, with or without solar disturbances, when the turbine is fed by the receiver and the alternator is connected to the grid;
State 5: Thermal Storage System charge by superheated steam from the receiver;
State 6: Operation with the turbine fed by the storage system when the solar radiation is below a technical minimum;
State 7: Load rejection when the electric power delivered to the network vanishes because of a failure of the grid.

The transitions between these states are illustrated in Fig. 19.

4. System example simulation results and analysis

Based on the components mathematical models discussed above, the whole CRS plant model is established in TRNSYS as shown in Fig. 20. It is mainly composed by the following models from TRNSYS library [8]:

Weather Data Processor (Type15): This component serves the purpose of reading data at regular time intervals from a data file and making it available to other TRNSYS components as time-varying forcing functions. It can calculate the solar zenith angle and azimuth angle at different time and sites. This output is used to interpolate the heliostat field efficiency matrix provided by user from the HFLD calculation results as shown in Fig. 10.
Heliostat Field (Type194): This model contains information including the field area, heliostats number, start-up and tracking electric power, field efficiency matrix and other operational limits.
Tower Receiver (Type195): Generally, the receiver model provides as output the flowrate required to achieve the outlet steam temperature and pressure set point. For plant's performance prediction based on energy balance, the flux distribution on receiver surface that calculated by HFLD is used to get the receiver efficiency curve as shown in Fig. 17. The various thermal losses are calculated and compared to some tested models as listed in literatures [12].
Power Cycle: It contains the models used in conventional power plant, like the turbine stages, turbine controller, condenser, deaerator, throttle, generator, pumps, etc. As the work presented mainly focuses on solar field performance, so those models in power cycle are not listed specifically here.

According to the recent 20 years' weather information data measured in Beijing, the TMY (Typical Meteorological Year) for the place where DAHAN locates is calculated and used in the plant model as weather input [13]. After comparison of the four kinds of heliostat field layout, the North-South staggered type (Fig. 6) is preferred for its low cost and high annual efficiency. The basic mass and energy balance flow of the whole CRS plant model in Fig. 20 is described in Fig. 4.

For estimation of average annual performance, the rating point for simulation was chosen at 12:00 on Mar 22nd which is Spring

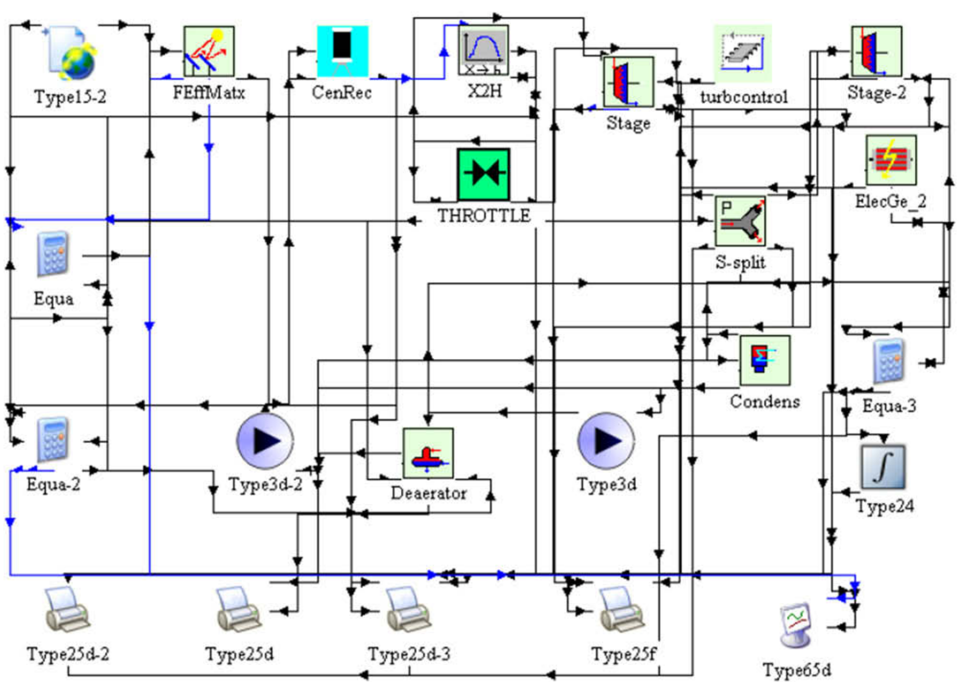

Fig. 20. DAHAN CRS plant model in TRNSYS.

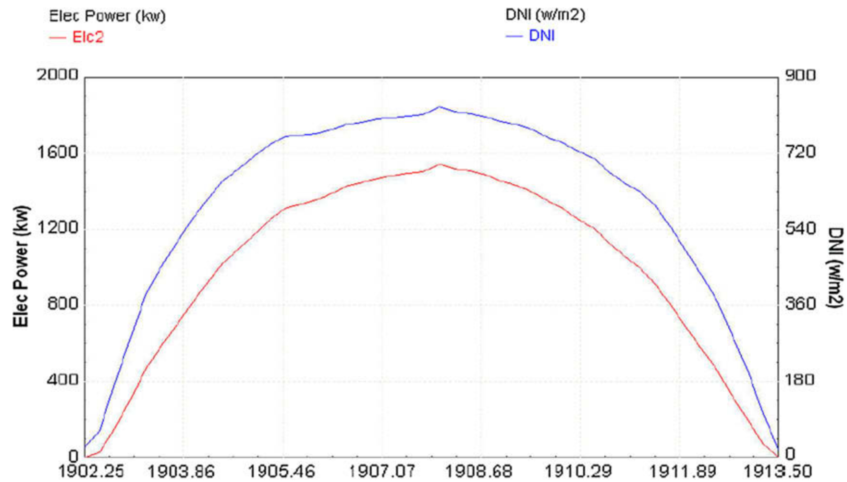

Fig. 21. Electricity power produced on the day simulated.

Equinox with DNI 830 W/m^2. The main plant operation mode that superheated steam from receiver outlet sent directly to turbine inlet is chosen for simulation prediction. It's assumed 100% heliostats are available to track the receiver and are canted properly. Ambient temperature of 25 °C and wind velocity of 4 m/s are chosen as boundary conditions for receiver's thermal losses calculation in operation. Considering the low capacity, the turbine's relative internal efficiency and mechanical efficiency are set as 0.69 and 0.98 separately. The mathematical relationship for the energy flow in this case is as follows in Equation (10):

$$E_{NET} = E_{AVAIL} \cdot \eta_{field} \cdot \eta_{REC} \cdot \eta_{EPGS} \cdot \eta_{NET/GROSS} \tag{10}$$

where, E_{AVAIL} is the daily incident thermal energy during times that fluid is flowing through the receiver; η_{REC} is the receiver efficiency; η_{EPGS} is the thermal efficiency of the electric power generation system; $\eta_{NET/GROSS}$ is the daily electric parasitic efficiency.

The thermal property parameters calculated for various points as shown in Fig. 3 are as follows:

Point 1: (Same as Point 13): $P = 2.354$ MPa, $T = 390\,^\circ$C, $H = 3219.34$ kJ/kg
Point 2: $P = 2.5$ MPa, $T = 400.0\,^\circ C$, $H = 3239.96$ kJ/kg
Point 3: $P = 0.0073$ MPa, $T = 39.784\,^\circ C$, $H = 2504.7$ kJ/kg
Point 4: $P = 0.0073$ MPa, $T = 39.78\,^\circ C$, $H = 166.64$ kJ/kg
Point 5: $P = 0.12$ MPa, $T = 41.0\,^\circ C$, $H = 171.82$ kJ/kg
Point 6: $P = 0.3$ MPa, $T = 210.04\,^\circ C$, $H = 2886.32$ kJ/kg
Point 7: $P = 0.12$ MPa, $T = 104.0\,^\circ C$, $H = 435.99$ kJ/kg
Point 8: $P = 2.75$ MPa, $T = 106.6\,^\circ C$, $H = 448.91$ kJ/kg
Point 10: $P = 2.43$ MPa, $T = 261.4\,^\circ C$, $H = 2914.09$ kJ/kg
Point 11: $P = 2.35$ MPa, $T = 220.7\,^\circ C$, $H = 2800.05$ kJ/kg
Point 12: $P = 2.35$ MPa, $T = 320\,^\circ C$, $H = 3110.76$ kJ/kg

From those data, the power cycle efficiency can be calculated. The daily electricity power generated to the changing DNI value is as shown in Fig. 21. From this simulation result, it can be found that there are about 7 h which can produce more than 1 MWe power capacity under the assumed typical daily weather. The calculated annual electricity production is shown in Fig. 22. It can achieve gross electrical energy of 3.22 GWh under the assumed annual meteorological basis [14]. The annual sum of DNI used for simulation here is around 2200 kWh/m^2 and the annual total solar to electric efficiency is 14.6% under the State 4 (Normal operation mode) with assumed 2700 h of annual sum operation. Those assumptions are acceptable for estimation on energy balance.

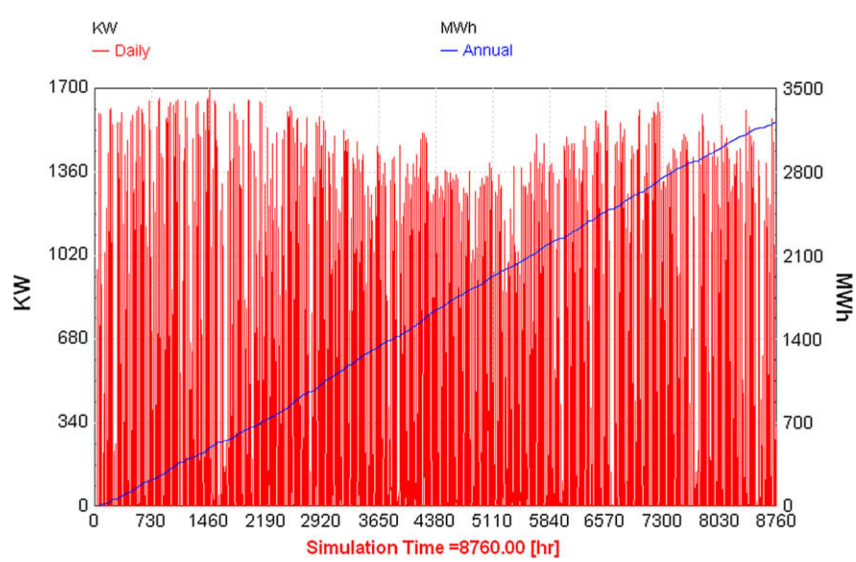

Fig. 22. Daily and annual electricity production in calculation for DAHAN.

5. Conclusions

Many papers related to CRS theoretical research and experimental tests have been presented since 1970s. Most of them focus on the various mechanisms analysis of plant components including heliostat, receiver and storage medium. The work described in this paper is about the mathematical models establishment of the main basic components in CRS and then their integration to be a whole plant model for simulation. The simulation results of a reference day with annual average DNI and the yearly generated electricity are shown. The work discussed here is all based on energy balance. The final objective of this work is to predict the transient behavior of the thermodynamic variables associated to the external disturbances and operational inputs change. More detailed receiver two-phase thermodynamic model combined with flux distribution information on surface panels need to be developed. The construction completion of DAHAN which is regarded as the milestone in China's solar thermal power development will provide a test base for various solar thermal power research. Also, the operating demonstration of DAHAN will enforce the solar thermal power commercialization in China which maybe have the world's widest renewable energy market potential.

Acknowledgements

This work has been financed by the China Ministry of Science and Technology under National High Technology Development "863" Plan with Project No. (2006AA050101). The authors want to acknowledge all participants' cooperation.

References

[1] State Electricity Regulatory Commission, People's Republic of China. Report: China's total installed capacity of electric power in 2007. See also: http://www.serc.gov.cn/xyxx/dljs/200802/t20080220_4962.htm.
[2] Garcia P, Ferriere A, Bezian JJ. Codes for solar flux calculation dedicated to central receiver system applications: a comparative review. Solar Energy March 2008;82(3):189–97.
[3] Final technical progress report – 10 MW solar thermal power plant for Southern Spain. Project funded by the European Community under the 5th framework programme (1998–2002). Partners: Solucar, DLR, Ciemat, Inabensa, Fichtner.
[4] PPT. PS10: a 11.0-MWe solar tower power plant with saturated steam receiver. See: http://www.upcomillas.es/catedras/crm/report05/Comunicaciones/Mesa%20IV/D.%20Valerio%20Fern%C3%A1ndez%20-%20Solucar%202.pdf.
[5] Stoddard MC, Faas SE, Chiang CJ, Dirks JA. SOLERGY – a computer code for calculating the annual energy from central receiver power plants. Sandia National Lab.; 1987.
[6] Faas SE, Winters WS. An evaluation of heliostat field/receiver configurations. Sandia report 86-8007. Sandia National Laboratory; 1986.
[7] Stine William B, Geyer Michael. Power from the Sun. See also: www.powerfromthesun.net; 2001.
[8] Schwarzbozl Peter, Eiden Ulrich. A TRNSYS model library for solar thermal electric components (STEC). A reference manual release 2.2; Sept. 2002.
[9] Baker AF, Faas SE, Radosevich LG, Skinrood AC, Peire J, Castro M, et al. U.S.–Spain evaluation of the solar one and CESA-1 receiver and storage systems. Sandia National Lab.; 1989.
[10] Siebers DL, Kraabel JS. Estimating convective energy losses from solar central receivers. SAND84-8717. Sandia National Laboratories; April 1984.
[11] Jacobs H. Receiver losses: results of tests. Draft report. Sandia National Laboratories; 1985.
[12] Yao ZH, Wang ZF. Theoretical simulation investigation of the pioneer 1 MW solar power tower system in China. In: Proceedings of solar world congress, vol. IV; 2007. p. 1733–7.
[13] JohnDuffie A, WilliamBeckman A. Solar engineering of thermal processes. 3rd ed. Hoboken, New Jersey: John Wiley & Sons, Inc.; 2006.
[14] Carasso M, Becker M. Performance evaluation standards for solar central receivers. In: Solar thermal central receiver systems, vol. 3. Berlin, Heidelberg: Springer-Verlag; 1990. Printed in Germany.